Proceedings of the Korean Nuclear Society Spring Meeting
Kori, Korea, May 2000

Development of Creep Constitutive Equation for Low Alloy Steel

Kwang J. Jeong, Joon Lim, Il S. Hwang
Seoul National University
Seoul, 151-742, Republic of Korea

ABSTRACT

High temperature creep tests of SA533B1 steel were performed under both constant load and constant stress conditions. Using the minimum creep strain rates as a function of the given stress and temperature conditions, simple power law type curve fittings were performed. Based on the results of curve fittings of constant stress data, creep constitutive law was developed. The constitutive law was then implemented in ABAQUS 5.8 and validated against Lower Head Failure (LHF) experiment executed in Sandia National Laboratories (SNL). The constitutive law was shown to be useful in predicting the lower head deformation behavior. Additional work, however, is needed to determine the correlation between the constant load data and constant stress data.

I. INTRODUCTION

The lower head of the reactor vessel can be subjected to significant thermal and pressure loads in the event of a core meltdown accident; consequently, the possibility exists that the lower head will fail releasing large quantities of core material to the containment. The mode, timing, and size of lower head failure are of prime importance in the assessment of core melt accidents because they define the initial conditions for ex-vessel events such as core/basemat interactions, fuel/coolant interactions, and direct containment heating. On the other hand, recent studies indicate that the deformation of a reactor vessel wall, leading to the possibility of in-vessel core retention without external cooling. Therefore, for both accident assessment and accident mitigation considerations, there is a need to develop a predictive capability of creep deformations and failure.

Furthermore international efforts to model the TMI-2 accident have generally predicted creep failure of the vessel, as it is well known, no failure or observable creep deformation occurred [1]. Therefore there has been a need for the accurate prediction model of both global and local deformations. Those deformations are important in defining the stress state and response of penetration welds, for instance, or in defining the boundary conditions that control failure initiation and propagation. A well-characterized material property database, for the actual materials used, is a primary requirement for the predictions.

Most creep data for SA533B1 steel under severe accident conditions is derived under constant load conditions which is performed by recording strain of tensile specimen with constant applied load at constant temperature. This is done because it is easy to perform in laboratory testing. The consequence of significant changes in the cross-sectional area of the specimen makes the stress higher than the initial value accelerating creep strain rates or initiating tertiary creep.

It assumes that the stress dependent terms in the creep constitutive law are the most troublesome from the convergence point of view. In tertiary creep, the stress exponent can be more than twice larger than the value of steady state creep making time steps smaller or the problem diverge. The cost of creep analysis is particularly high in three dimensional calculations. However, a more critical factor is that considerable user judgement is involved in deciding an appropriate hardening law concerning the stress and temperature changing conditions. Therefore from the points of view described above, it is very useful to use the creep constitutive law composed of only steady state creep.

In this study, creep tests of SA533B1 steel were performed under both constant load conditions and constant stress conditions, which are compared to each other. The main objective was to develop a creep constitutive law of SA533B1 steel composed of steady state creep only based upon constant stress creep data. The creep constitutive law developed can be used to predict vessel deformations under severe accident conditions.

II. EXPERIMENTS

II.A. APPARATUS

As a creep test frame, servo-hydraulic materials testing system (INSTRON 8516-100 kN) with a single zone wire wound split furnace and with a high temperature extensometer was used. To measure the temperature of the specimen, a K-type thermocouple was installed to the specimen with mechanical junction like American Society for Testing and Materials (ASTM) Method E 633 [2]. The load cell was calibrated to an accuracy of ±0.15 kN. Test specimen is 6.25 mm in diameter round specimen (modified ASTM Method E 8-93 [3]).

For high-temperature testing of materials which are readily attacked by their environment (such as oxidation of metal in air), the specimen may be enclosed in a capsule so that it can be tested in a vacuum or inert gas atmosphere. In this study as another way to avoid high surface oxidation on test specimens at these elevated temperatures, protective plating has been used. Instead of vacuum or inert gas atmosphere, plating was chosen because vacuum or inert gas chamber including high-temperature extensometer makes the testing apparatus too complicated if the same accuracy is to be retained.

Electrolytic nickel plating method was adopted. Specimen with 30 μm thickness of electrolytic nickel plating showed good resistance to high-temperature oxidation and stress-strain curve of it showed limited deviation from its original (non-plated) specimen [4].

II.B. TEST METHODS

Twelve constant load creep tests were performed with temperatures raging from 873 to 1023 K and times to rupture ranging from 30 minutes to 12.4 hours. During the tests, although the applied load remains constant through the tests, the stress of the specimen increases progressively as the cross-sectional area decreases. The stress of constant load test is usually denoted by its initial value, which is defined by the applied load divided by specimen initial cross-sectional area.

$$\sigma_0 = \frac{F_0}{A_0} \tag{1}$$

While the true stress in the test varies according the actual cross-sectional area, A,

$$\sigma = \frac{F_0}{A} \tag{2}$$

Nine constant stress creep tests were performed with temperatures ranging from 873 to 973 K and times to rupture ranging from 2.3 to 24.2 hours. In this case, the applied load is adjusted as the length of the specimen changes to maintain constant stress on the specimen. Constant stress conditions can be created by special test systems which automatically modify the applied load in proportion to the change in specimen cross-sectional area that is determined from the total accumulated strain assuming the constancy of specimen volume and the uniformity of deformation. This was achieved by employing servo-feedback systems for load control so that load was reduced progressively as strain accumulates. If we assume the volume constancy during the test, relation between the area of cross section and the length of the specimen is as follows:

$$A_0 L_0 = AL \tag{3}$$

and the definitions of the nominal and true strain are given,

$$\varepsilon_n = \frac{L - L_0}{L_0} \tag{4}$$

$$\varepsilon = \ln(\varepsilon_n + 1) \tag{5}$$

From the equations 3 to 5, cross section of the specimen during the test is given as follows:

$$A = A_0 \exp(-\varepsilon) \tag{6}$$

and the true stress is stated as,

$$\sigma = \frac{F}{A} \tag{7}$$

To maintain the initial stress of equation 1, the applied load F then can be determined from the eqtions 7 and 8,

$$F = F_0 \exp(-\varepsilon) \tag{8}$$

II.C. TEST RESULTS

Figure 1 shows the constant load creep data as a function of time in a given temperature and stress condition. Large part of the strain in each curve seems to be composed of accelerating strain or tertiary creep. Compared to the constant load data, nine curves of constant stress data as depicted in figure 2 show fairly long linear portion or steady state creep. Both tests of constant load and constant stress show negligible primary creep regime.

Failure under constant stress conditions eventually occurs due to some microstructural and/or mechanical instability in the same manner as, but much later than, constant load tests. Once a local variation in cross-sectional area is formed, the actual stress is higher than the imposed constant stress and further deformation concentrates at the location. In reality, the basic assumptions of conservation of volume or uniform deformation have been violated. When non-uniform deformation starts in either a constant load or constant stress test, the local strain and strain rate vary along the gage section in an unknown manner [5]. Table I summarizes the detailed test data including test conditions, rupture time, and minimum creep strain rates.

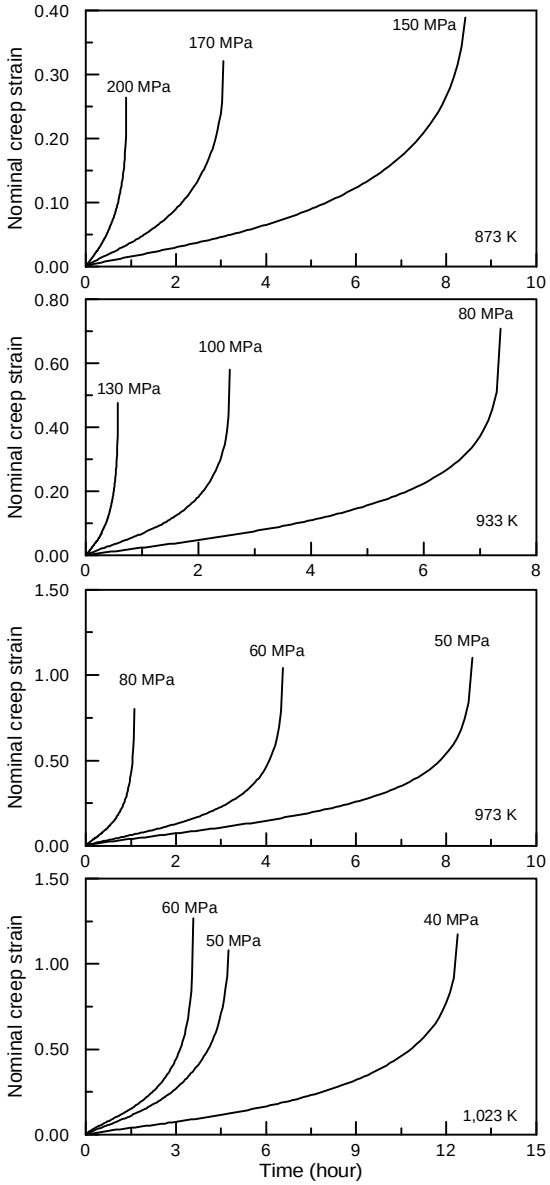

Figure 1. SA533B1 creep test curves at constant load conditions

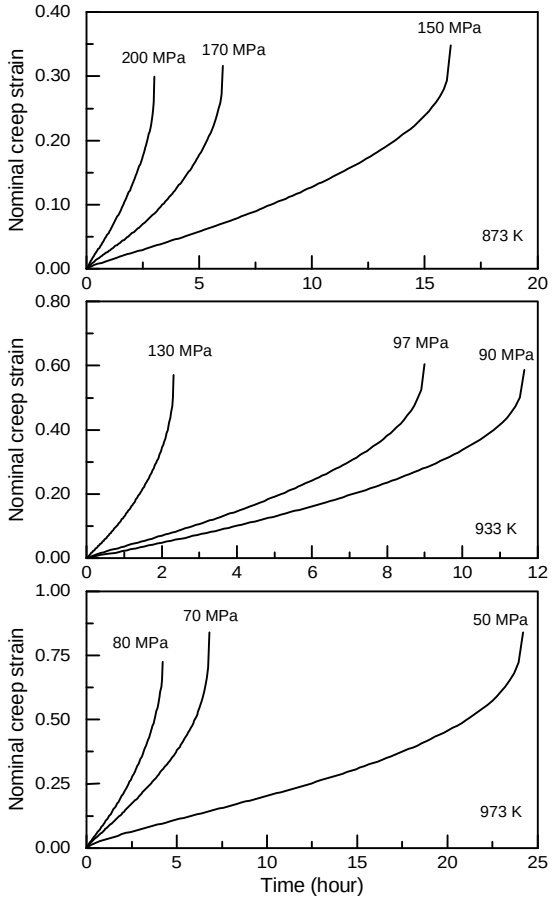

Figure 2. SA533B1 creep test curves at constant stress conditions

Table I. SA533B1 creep data

No.	Temp. (K)	Stress (MPa)	Normalized stress ($\sigma/\sigma_y(T)$)	Rupture time (h)	$\dot{\varepsilon}_{min}$ (h^{-1})	comment
1	873	150	0.769183	8.433333	0.015732	
2	873	170	0.871741	3.051667	0.03816	
3	**873**	**200**	**1.025577**	**0.896389**	**0.10296**	**$s_0 > s$**
4	933	80	0.60928	7.373611	0.025164	
5	933	100	0.7616	2.561667	0.06984	
6	933	130	0.99008	0.567778	0.24012	
7	973	50	0.502516	8.585834	0.03636	
8	973	60	0.60302	4.374166	0.06336	
9	973	80	0.804026	1.071667	0.21816	
10	**1023**	**40**	**0.559141**	**12.39111**	**0.026064**	**T > 1000 K**
11	**1023**	**50**	**0.698926**	**4.743611**	**0.07596**	**T > 1000 K**
12	**1023**	**60**	**0.838711**	**3.579167**	**0.10872**	**T > 1000 K**
13*	873	150	0.769183	16.15278	0.011952	
14*	873	170	0.871741	6.035833	0.028296	
15*	**873**	**200**	**1.025577**	**2.995278**	**0.05976**	**$s_0 > s$**
16*	933	90	0.68544	11.65611	0.025776	
17*	933	97	0.738752	8.995	0.03636	
18*	933	130	0.99008	2.316111	0.1314	
19*	973	50	0.502516	24.20194	0.020772	
20*	973	70	0.703523	6.791945	0.06948	
21*	973	80	0.804026	4.207222	0.1026	

*: constant stress data
note: bolded data excluded from curve fitting process

III. CURVE FITTINGS

The traditional approach to correlating creep is to fit a power law function of the form

$$\varepsilon = A(T)\sigma^m t^n \tag{9}$$

to the experiment data. Under severe accident conditions, the quantity A(T), which is of mixed dimensions, is a hypersensitive function of temperature. The exponent *n* is taken as unity to represent steady state creep rate or minimum creep rate,

$$\dot{\varepsilon} = A(T)\sigma^m \tag{10}$$

Given the mixed-dimensional nature of A(T) and its sensitivity to the temperature, an alternate formulation of equation 11 was explored. First, Arrehnius type temperature dependent term was added. And to normalize the stress term, stress term was divided by temperature dependent yield strength. Optimal results were obtained with a creep model of the form,

$$\dot{\varepsilon} = \frac{1}{t_{ref}}\left(\frac{\sigma}{\sigma_y(T)}\right)^m e^{-\frac{T_{ref}}{T}} \tag{11}$$

The temperature dependent yield strength is suggested by Reference 6.

$$\sigma_y(T) = \frac{\sigma_{ref}}{1 + \left(\frac{T}{T_{ref}}\right)} \tag{12}$$

where, σ_{ref} = 477.95, T_{ref} = 837.66, and c = 9.0062, for T <= 950 K,
and σ_{ref} = 5129.1, T_{ref} = 541.52, and c = 6.6944, for T > 950 K

Each linear portion of the creep curve (in the form of strain vesus time) in the database was fit with a straight line,

$$\varepsilon = \dot{\varepsilon}_{min} t \tag{13}$$

Here $\dot{\varepsilon}_{min}$ is physically interpreted as the minimum creep rate and its definition is denoted as follows,

$$\dot{\varepsilon}_{min} = A(T)\sigma_0^m = \frac{1}{t_{ref}}\left(\frac{\sigma_0}{\sigma_y(T)}\right) e^{-\frac{T_{ref}}{T}} e^{\pm\sigma_{err}} \tag{14}$$

where σ_0 is the stress at the beginning of the test. Uncertainties in the fittings are represented by a root-mean-squared (RMS) error defined by

$$\sigma_{err} = \left\{ \frac{\sum_{i=1}^{N} \left[\ln(\varphi_{p,i}) - \ln(\varphi_{m,i})\right]^2}{N-1} \right\}^{1/2} \tag{15}$$

where the RMS error is defined in terms of the natural logs of curvefit predictions ($\varphi_{p,i}$) and data measurement ($\varphi_{m,i}$). The natural log is requred because each material property exhibits order-of-magnitude variations on the temperature range of interest, and the errors are normally distributed in this format. Uncertainties in the creep strain rate equations are reflected by the factor $e^{\pm\sigma_{err}}$. Curve fittings were performed according to equation 14. Commercially available curvefitting software was used to determine the constants t_{ref}, m, and T_{ref} in the creep constitutive law. The data points where $\sigma_0 / \sigma_y(T) \geq 1.0$ are excluded because $\dot{\varepsilon}_{min}$ would then reflect a bootstrap relationship between creep deformation and plastic deformation. Data points where T > 1000 K are also excluded not to include phase transformation phenomenon. Table I summarized the compilation of $\dot{\varepsilon}_{min}$ as a function of normalised stress, $\sigma_0 / \sigma_y(T)$ and temperature, T. Table II summarizes the fitting parameters calculated. The r-squared value of the fitting, r^2, and uncertainties of the each fitting are also depicted in the table.

Table II. Curve fitting parameters

parameters	constant load	Constant stress
t_{ref}	2.500E-09	2.401E-07
m	4.278E+00	3.861E+00
T_{ref}	1.981E+04	1.615E+04
r^2	0.967	0.953
σ_{err}	0.134	0.137

Using equations 1-5, the time-dependent true stress, σ, can be written as

$$\sigma = \sigma_0 e^{\varepsilon} \tag{16}$$

for the special case of a constant load, uniaxial creep test, with constant temperature. Here σ_0 is the stress in the specimen before significant elongation occurs. Increasing elongation causes the true stress to increase because the cross-sectional area decreases while the load is held constant. An analytic solution of equation 15 can be

obtained by integrating equations 10 using equations 14 and 16 for the special conditions noted above,

$$\varepsilon = -\frac{1}{m}\ln(1-t^*) \tag{17}$$

where,

$$t^* = tm\frac{1}{t_{ref}}\left(\frac{\sigma}{\sigma_y(T)}\right)^m e^{-\frac{T_{ref}}{T}}$$

The analytic solution suggests that the constant load creep database should collapse to a single curve if plotted in the nondimensional coordinates of ε versus t* using equation 17. While using equation 13, ε versus t* relations of constant stress data is as follows:

$$\varepsilon = \frac{1}{m}t^* \tag{18}$$

The analytic solution also suggests that the constant stress database should collapse to a single curve if plotted in the nondimensional coordinates of ε versus t* using equation 18.

To define t*, parameters of constant stress data in table II are used. Figure 3 shows the ε versus t* curves. The results show well collapsed behavior between the test data curves and their analytic function in case of constant stress case except later part of their curves. Accelerated strain behavior in later part of each curve in constant stress case may come from localized necking or microstructural damages. Those later parts can be neglected by the assumption that those instabilities come after significant deformations. Besides it is not explained why the constant load data show more creep strain, in figure 3, than expected from the analytic master curve calculated from constant stress data.

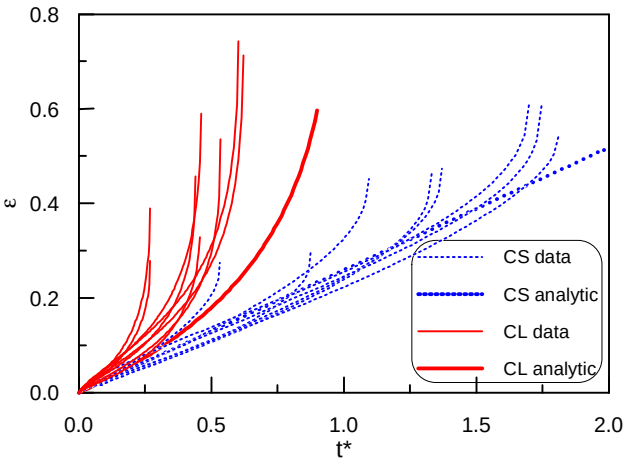

Figure 3. Plots of analytic functions and creep database in normalised axes
(CS data: constant stress data, CS analytic: analytic function of constant stress data, CL data: constant load data, and CL analytic: analytic function of constant load data)

IV. VALIDATION TO THE EXPERIMENT

IV.A. DESCRIPTION OF LHF TESTS

LHF test of U.S. Nuclear Regulatory Commision (NRC) was chosen to validate the creep constitutive law [6]. The LHF experimental program consisted of a series of eight experiments. They were designed to examine the effects of spatial temperature/heat flux distribution, pressure, and reactor vessel structure elements and construction features on RPV deformation and failure. The first test among them, LHF-1, was chosen as the validation case which test was already shown to be amenable to modeling by its replicate tests[6].

Figure 4 shows the temperature history of the inside vessel as a function of lattitude (90 latitude denotes the bottom apex of the vessel) and also shows the pressure history of the vessel. Vessel outside temperatures are about 10 K lower than the inside values. The nominal vessel outer diameter was 0.91 m and figure 5 shows three dimensional thickness map of the vessel.

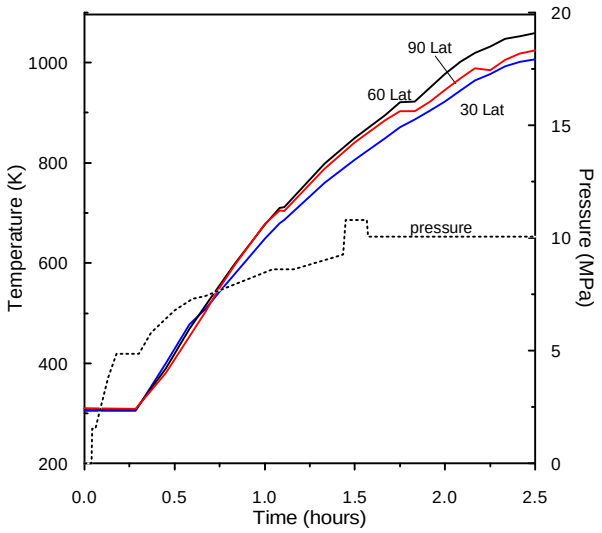

Figure 4. Temperature histories as a function of latitude and pressure history of LHF-1

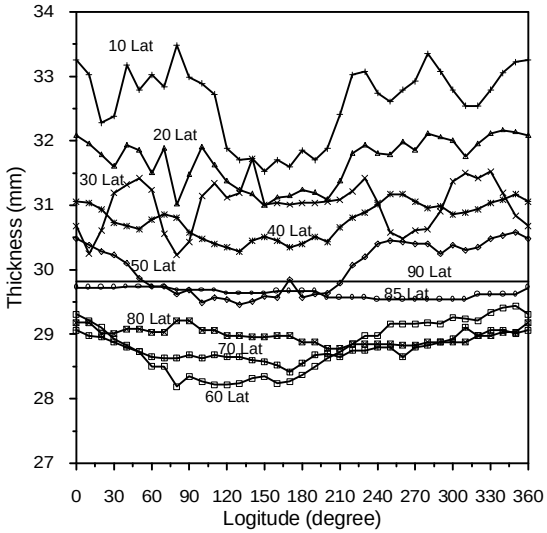

Figure 5. Three dimensional wall thickness map

IV.B. CREEP CONSTITUTIVE LAW

The experiment was modeled with both axisymmetric elements and three dimensional elements. Axisymmetric elements were used for computational efficiency even though the thickness and temperature distributions in the tests varied slightly form a true axisymmetric model. The axisymmetric model is believed for the identifying the parameters that affect vessel deformation and for predicting vessel deformation to first order. Latitudinal variations of the vessel thickness were explicitly modeled according to the vessel failure locations. The lower head was modeled with 90 elements (one for each angular degree) and five radial elements, for a total of 450 elements. In ABAQUS, the computational elements were defined as a "CAX8R," which are eight noded quadrilateral elements with reduced integration [7]. This nodalization gives accurate resolution to the stress gradients expected in the analyses.

In the experiments, the hemisphere was cooled near the equator where it was welded to a thick cylidrical shell. The computational model simulated this boundary condition by restraining the equatorial nodes so that they could not move vertically or radially. A pressure boundary conditon was established on the inside surface elements. A separate temperature history was specified for each of the 450 computational elements. The temperature histories were established by selecting the hottest array of latitudinal measurements made on the inside of the vessel as shown in figure 4. Tensile properties (E, ν, σ_y, E_p, σ_u) are input to ABAQUS. The creep model was specified with a user subrouitine that returns the creep strain rate as a function of the instantaneous temperature and stress states.

To examine three dimensional thickness variation effect on the deformation behavior, analysis with three dimensional elements was also performed. Before the analysis, mesh sensitivity tests were executed to reduce the number of elements as much as possible. With the same eight noded quadrilateral axisymmetric elements, 9 elements and 1 radial element gave almost the same results of the previous 450 elements. Based on the sensitivity results, 9 elements, 1 radial element, and 36 longitudinal elements, for a total of 324 elements were used, as the three dimensional analysis. Thickness variation to the longitudinal angle, as well as the latitude variation was implemented in three dimensional model. In ABAQUS, the computational element was defined as a "C3D20," which are 20 noded three dimensional quadrilateral elements. The boundary conditions including the temperature conditions were used as the same method as used in the axisymmetric case. Consequently three dimensional analysis is representing the result which has the effect of longitudinal thickness variations compared to axisymmetric model.

Vertical displacement of the lower head is a fundamental measurement in the LHF tests against which model predictions can be compared. Displacements are observed to occur in two phases: the first is characterized by small displacement rate and the second is characterized by a large and accelerating displacement rate. The period of small displacement rate is associated with thermal expansion and elastic displacement as the vessel heats up and is pressurized. The second phase for displacement is characterized by large and accelerrating deformation rate and is of greater intest in severe accident assessments. Figures 6 shows the deformation behavior of axisymmetric model and figure 7 shows the deformation behavior of three dimensional model. The ABAQUS models accurately predicted both displacements of axisymmetric case and three dimensional case during the early phase as well as the large deformation behavior.

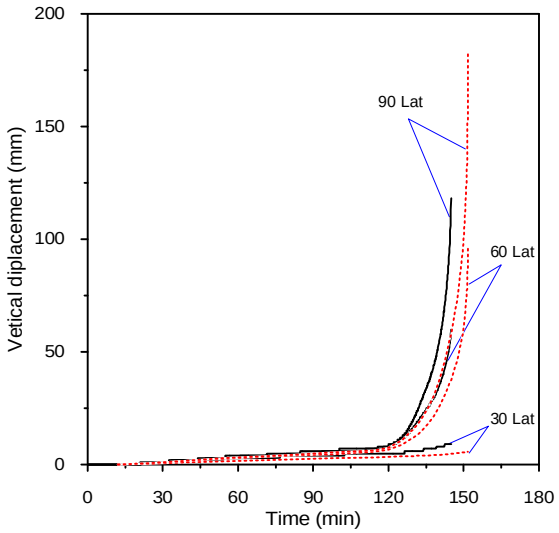

Figure 6. Displacements of LHF-1 (solid lines represent represent experiments and dashed lines represent axi-symmetric modeling results)

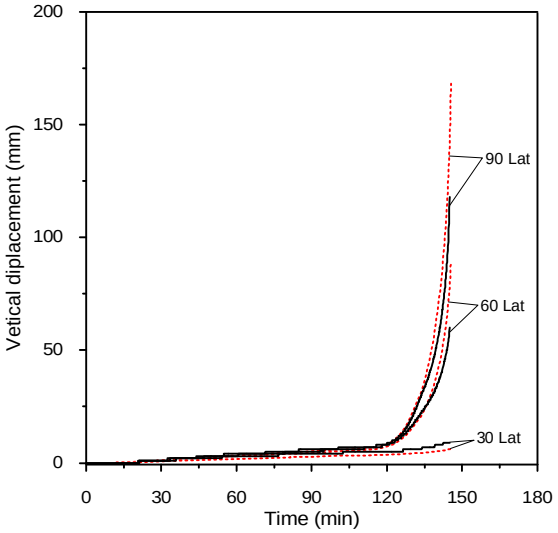

Figure 7. Displacements of LHF-1 (solid lines experiments and dashed lines represent three dimensional modeling results)

V. CONCLUSIONS

Finite element analyses have played an important role in lower head structural analyses since the time of TMI-2. However, analyses of the TMI-2 accident, as part of the OECD/TMI-2 VIP project, generally predicted failure of the RPV lower head when failure obviously did not occur [1]. Since then there have been a number of international programs on creep deformation and rupture behavior.

Most creep data for SA533B1 steel under severe accident conditions is derived under constant load condition which is performed by recording strain of tensile specimen with constant applied load at constant temperature. The consequence of significant changes in the cross-sectional area of the specimen makes the stress higher than the initial value. To incorporate such creep data into the model, there has been numerous approaches such as continuum damage mechanics, theta projection method, etc. While there have been efforts to use minimum creep rate only with the assumption that tertiary creep comes from mainly the local area reduction corresponding the local higher stress concentration [6]. In that case the implementation of the creep constitutive law to the finite element analyses can be much more simplified. There is a need to execute the constant stress test to confirm the assumption. Nine constant stress test were performed from the archive material of the LHF test, and twelve constant load creep tests were also performed to find out the correlation between them. The constant stress data confirms that steady state creep is maintained during the most part of the experiment if the applied load is adjusted to held constant stress of the specimen. However, additional work is needed to determine the correlation between the constant load data and constant stress data.

The constitutive law of SA533B1 developed in this study:

1. is mainly based on the assumption that there is no or little tertiary creep in SA533B1 if the load can be adjusted so that the stress is maintained constant,
2. has no tertiary creep which often causes numerical divergence problem because of the higher stress exponent, and
3. has no need to decide a certain hardening law, such as time hardening or strain hardening, should be used .

And the results of validation against LHF test show well predicted results in both axisymmetric and three dimensional cases.

NOMENCLATURE

A_0	initial cross section of the specimen (m^2)
A	cross section of the specimen (m^2)
A(T)	temperature dependent coefficient
$\dot{\varepsilon}_{min}$	minimum creep strain rate (1/h)
$\dot{\varepsilon}$	strain rate (1/h)
ε_0	nominal strain
ε	true strain
E	elastic modulus

E_p	plastic modulus
F_0	initial applied load (MPa)
F	applied load (MPa)
L_0	initial length of the specimen (m)
L	length of the specimen (m)
m	stress exponent
n	time exponent
N	number of data points
φ_m	data measured
φ_p	data predicted
$\sigma_y(T)$	yield strength (MPa)
σ_0	nominal stress (MPa)
σ	true stress (MPa)
σ_{err}	standard error deviation
T_{ref}	temperature constant (K)
T	temperature (K)
t_{ref}	time constant (h)
t	time (h)
t*	nondimensionalized time

REFERENCES

1. L.A. Stickler, et al., Calculations to Estimate the Margin to Failure in the TMI-2 Vessel, NUREG/CR-6196, TMI V(93) EG01, EGG-2733, Idaho National Engineering Laboratory, 1994
2. ASTM, Standard Guide for Use of Thermocouples in Creep and Stress Rupture Testing to 1000 ºC (1800 ºF) in Air, ASTM Standards E 633-87, Annual Book of ASTM Standards, 1987
3. ASTM, Standard Test Methods for Tension Testing of Metallic Materials, ASTM Standards E 8-93, Vol. 03.01, Section 3, Metals Test Methods and Analytical Precedures, 1993
4. D.C. Lim, Study on the Creep Behavior of SA508 Cl.3 at Elevated Temperature, Master' s Thesis, Department of Nuclear Engineering, Seoul National University, 1998
5. ASM, Creep, Stress-Rupture, and Stress-Relaxation Testing, Metals Handbook, Vol. 8, Mechanical Testing, 1985
6. T.Y. Chu, et al., Lower Head Failure Experiments and Analyses, NUREG/CR-5582, 1999
7. Hibbit, Karlsson & Sorensen, Inc., ABAQUS User's Manual, Version 5.8, Providence, Rhode Island, 1998